Holographic optical elements (HOEs) for true-time-delays aimed at phased array antenna applications

Ray T. Chen and Richard L.Q. Li
Microelectronics Research Center
Department of Electrical and Computer Engineering
The University of Texas at Austin, Austin, Texas 78712
Phone:(512)471-4349; Fax:(512)471-8575 Email: raychen@uts.cc.utexas.edu

ABSTRACT

True-time-delay beam steering in optical domain for phased-array antenna applications using multiplexed substrate guided wave propagation is introduced. Limitations of practical true-time-delays are discussed. Aspects on making holographic grating couplers are considered. Finally, experimental results on the generation of 25 GHz broadband microwave signals by optical heterodyne technique and 1-to-30 massive substrate guided wave optical fanout with an uniform fanout intensity distribution are presented.

1. INTRODUCTION

Phased-array antenna (PAA)s offer many advantages, including steering without physical movement, accurate beam pointing, increased scan flexibility, precise elemental phase and amplitude control to obtain low spatial sidelobes, and reduced power consumption and weight. PAA systems combine the signals from as many as thousands of antenna elements to point a directive beam at some angle in space. The characteristics and angle of the beam are selected electronically across the array elements using analog or digital control of the amplitude and phase of excitation. Such an electronic phase control is accomplished through bulky, heavy coaxial waveguide feed. Furthermore, as higher frequency phased array operation is pursued, element spacing will become increasingly tight, making waveguide congestion and crosstalk at the array backplane serious concerns. With the progress in photonic technology, most of these control functions can be performed by photonic systems[1]. For instance, photonic systems can be used to provide true-time-delay(TTD) transmission paths for the microwave signals that are distributed to array elements[2].

Here , the distribution of true-time-delay broadband microwave signals for phased array antenna through massive substrate guided waves combined with surface-normal coupling are presented. The broadband microwave signals are generated through optical heterodyne technique. The physical aspects of phase-shifters and true-time-delay are first introduced. Then design issues on the photonic TTD architecture and related topics are addressed. Principle and practical constraints on making holographic grating couplers are discussed next, especially concerning with recording gratings on DuPont photopolymer materials. Finally, the generation and detection of high frequency microwave signals up to 25 GHz by optical heterodyne techniques are illustrated. A 1-to-30 massive fanout based on a multiplexed waveguide hologram is further demonstrated at 514 nm with energy variation within ±3%. Perspective overall system merit and obstacles on realizing the device are briefly explained as well.

0-8194-2063-8/96/$6.00

2. PHASE SHIFTERS AND TRUE-TIME-DELAY CONTROL

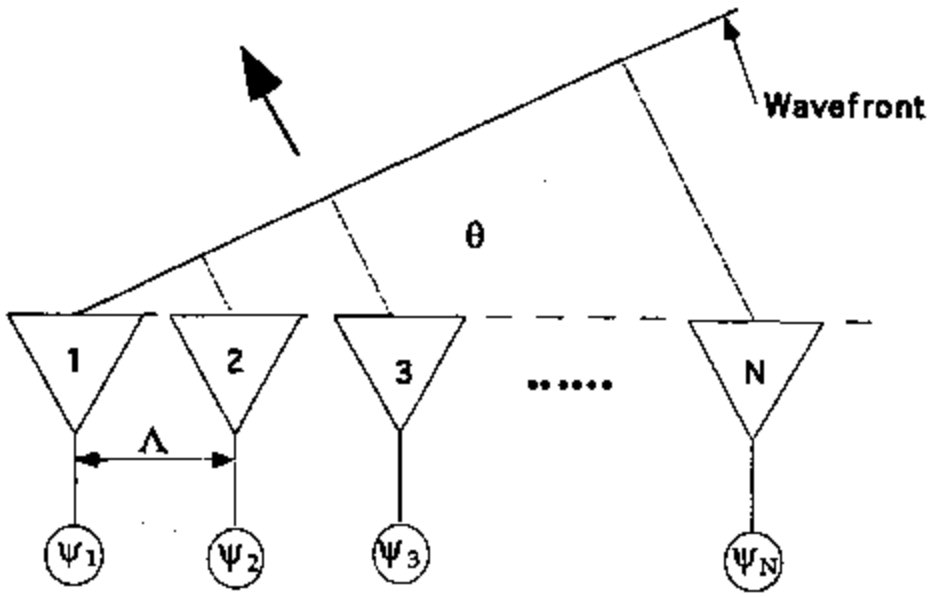

Figure 1 Phase array antenna phase shifter control

As illustrated in Fig. 1, for a linear array radiating elements with individual phase control, the far field pattern along the direction of θ_0 can be expressed as

$$E(\theta,t) = \sum_{n=0}^{N} a_n \exp(i\omega_m t)\exp[i(\psi_n + nk_m \Lambda \sin\theta)] \tag{1}$$

where ω_m is the microwave frequency; $k_m = \omega_m / c$ is the wave vector, and Λ is the distance between radiating elements. By electronically controlling the relative phase between successive radiating elements of the array, the direction of the radiated beam can be steered. For example, to point the beam at an angle θ_0, ψ_n is set to the following value

$$\psi_n = -nk_m \Lambda \sin\theta_0. \tag{2}$$

Differentiating the above equation, we have

$$\Delta\theta_0 = -\tan\theta_0 \left(\frac{\Delta\omega_m}{\omega_m} \right). \tag{3}$$

It is clear that for a fixed set of ψ_n's, if the microwave frequency is changed by an amount $\Delta\omega_m$, the radiated beam will drift by an amount $\Delta\theta_0$. This phenomenon is called "beam squint", which leads to an

undesirable drop of the antenna gain in the θ_0 direction. To satisfy the wide bandwidth requirements of future PAAs, true-time-delay (TTD) steering techniques must be implemented so that the far field pattern is independent of the microwave frequency.

In the TTD approach, the path difference between two radiators is compensated by lengthening the microwave feed to the radiating element with a shorter path to the microwave phase-front. Specifically, the microwave exciting the (n+1) th antenna element is made to propagate through an additional delay line of length $D_n = nL(\theta_0)$. The length of this delay line is designed to provide a time delay

$$t_n(\theta_0) = (n\Lambda \sin\theta_0)/c \tag{4}$$

for the (n+1)th delay element. For all frequencies ω_m, ψ_n is given by

$$\psi_n = -\omega_m t_n(\theta_0). \tag{5}$$

With such a delay set-up, when the second phase term inside Eq. (1) is changed due to frequency "hopping", the first term will change accordingly to compensate for the change such that the sum of the two remain unchanged. Thus, constructive interference can be obtained in the direction θ_0 at all frequencies. Even there is an instantaneous change in microwave frequency, the radiated beam will maintain its specific angular direction.

3. PRACTICAL TTDs

TTDs permit greater bandwidth and hence higher resolution phased array radar operation than what is possible using electronic phase shifters. However, TTDs are not easily realized in practice. Notice that by setting the various time delays according to Eq. (4) we only achieved "squint-free" beam forming at one specific beam pointing direction θ_0. In order to scan the beam into another angle θ', a completely different reconfiguration of the delays has to be established. The total number of delay configurations is determined by the maximum steering angle and the minimum angular scan resolution. Obviously, this can be a very large number if continuous true-time-delay are required. In practice, a total number of $R=2^N$ discrete delay lines (called N-bit delay) is constructed as the time-delay unit. This approximation may introduce sidelobe errors. Since practical PAA array elements K can be as high as 10,000, this results in a very large number ($R\times K$) of total delay lines. Therefore, straightforward implementations of TTD results in large hardware complexities and are impractical. Architecture must compress the hardware with respect to the number of delays per PAA element. One approach to reduce the number of delays is dividing the radiating elements into several subarrays and using "time steering" for only the subarrays. Each subarray behaves as a smaller antenna that can be individually steered with phase shifters over a reasonably wide bandwidth. We may regard such a system as a hybrid system with both TTD and phase steering.

In short, for a practical TTD beam steering system, two types of simplifications are usually necessary. First, array elements are divided into subarrays, each subarray share a common time delay network. In another words, not every array element owns a separate dedicated time-delay unit. Second, each time-delay unit is also built with discrete time delay increments. The delay selected for each steering angle represents a "quantized" approximation to a linear phase taper that dictates delay times of $0, \Delta t, 2\Delta t, \bullet\bullet\bullet, N\Delta t$ across the array, where Δt is given by $\Lambda \sin\theta_0 / c$. In this way, the system provides some, but not all, of the benefits of true-time-delay steering.

Hughes research laboratory[3] demonstrated a true-time-delay unit that consists of eight fiber delay lines which form 2^3 discrete delay increments $(0, \Delta t, 2\Delta t, \bullet\bullet\bullet, 7\Delta t)$ for achieving three bits of resolution in setting the microwave phase front. The radiating elements are grouped into four subarrays and the total number of TTD modules is four. The lengths of the fibers in these links were cut to provide a prespecified set of differential time delays determined by the antenna aperture and its maximum steering angle (θ_{max}). During steering of the phased array, one delay line, as specified by the steering angle, is selected from each of four such modules to provide time delay for the antenna subarray fed by the module. For example, when the antenna is programmed to steer to 16°(see Fig. 2), the specific time delays selected from the four time-shifters modules are respectively[4], $4\Delta t, 3\Delta t, \Delta t, 0$. Where Δt is the smallest differential delay increment in each module corresponds to the least significant bit of the three-bit approximation. Specifically, this minimum time interval is given by $\Delta t = L' \sin\theta_{max} / 7c$ for a 3-bit approximation, where L' is the separation between the center of the first and fourth subarray. The time delay from the first subarray to the phase-front at 16° is $\Delta\tau_1 = L' \tan 16° / c$, which is $7*\tan 16° / \sin\theta_{max}$ times the minimum delay Δt. For $\theta_{max} = 28°$ this is $4.27\,\Delta t \sim 4\,\Delta t$. The second subarray should have a time delay $\Delta\tau_2 = (2/3)L' \tan 16° / c$, which is $2.85\,\Delta t \sim 3\,\Delta t$. The third subarray should have a time delay $\Delta\tau_3 = (1/3)L' \tan 16° / c$, which is $1.41\,\Delta t \sim 1\,\Delta t$. The fourth delay obviously is zero.

The antenna beam was programmed to steer in the $+\theta_0$ or $-\theta_0$ direction by imposing the time delay code for θ_0 in the appropriate order across the array. For example, if the delay code for steering to +16° was $(4\Delta t, 3\Delta t, \Delta t, 0)$ then the corresponding code for -16°was $(0, \Delta t, 3\Delta t, 4\Delta t)$. The accuracy of this

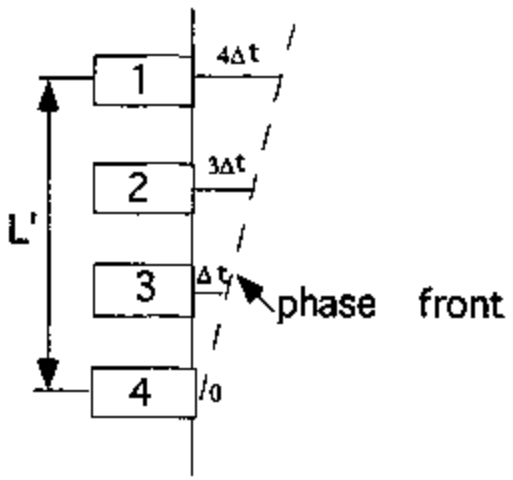

Figure 2. Programmed time-delays from the 4 modules for a 16° radiation

step approximation also limits the angular resolution---minimum angular step size ($\Delta\theta_{step}$)-- for steering the beam. At the steering angle θ_0, $\Delta\theta_{step}$ is approximately $(c\Delta t) / (L' \cos\theta_0)$. If the linear phase taper were approximated to a higher degree of accuracy with a smaller Δt, i.e., with more bits of resolution, then the antenna can be scanned at correspondingly smaller angular increments.

4. SUBSTRATE FANOUT TTD APPROACH

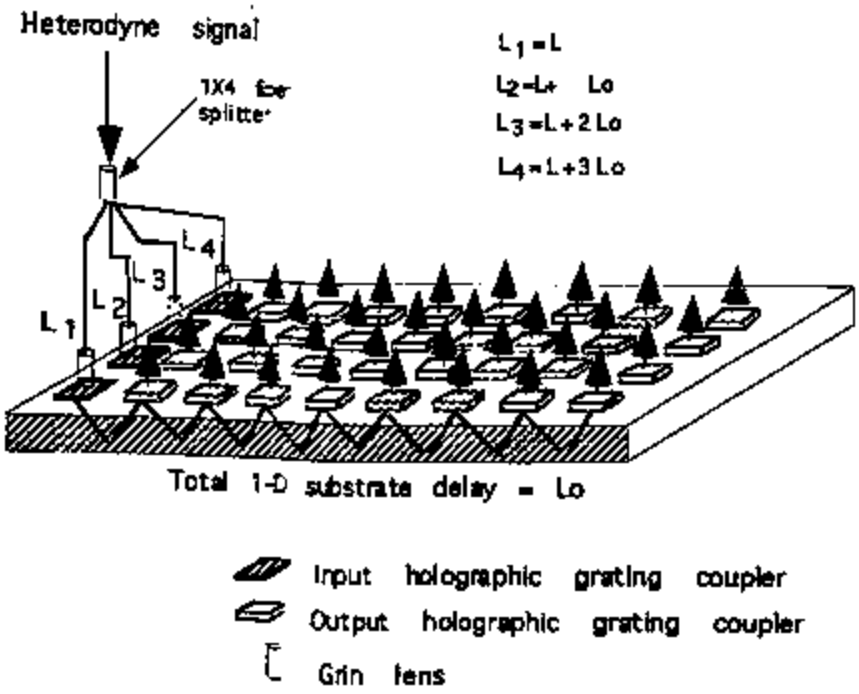

Figure 3 True-time-delay with substrate mode optical fanout

Figure 3 illustrates a proposed 2-D substrate mode guided wave optical elements used for massive fan-out true-time-delays with 5-bit resolution. Successive delays of 0, $\Delta\tau$, $2\Delta\tau$, $3\Delta\tau$, ...,$31\Delta\tau$ are provided by substrate-guided wave propagation with different bouncing distances. Let us look at some of the design issues. Suppose that the PAA is programmed to steer in the +45° to -45° direction range, i.e., $\theta_{max} = 45°$. For a 5-bit true-time-delay unit, the smallest differential delay increment $\Delta\tau$ corresponds to the least significant bit of the 5-bit approximation. This is given by

$$\Delta\tau = L' \sin\theta_{max} / 31c, \tag{6}$$

where L' is the dimensional size of the linear PAA. With a microwave center frequency of 30 GHz, the spacing between successive element is 5 mm and assume L'= 62 cm, then $\Delta\tau$ = 47ps. With a substrate total internal bouncing angle of 45°, the optical delay between successive output couplers is given by

$$\Delta t = \frac{\Delta L}{c/n} = \frac{2d/\cos\theta}{c/n}, \tag{7}$$

where d is the substrate thickness, c the speed of light, and n the index of refraction of the substrate material. From Eq.(6) and (7), it is found that d is approximately 3.3 mm.

5. HOE-BASED TRUE-TIME-DELAY

Optical fanout of various delay lines are accomplished by holographic volume phase grating couplers. These gratings couple the light into and out of substrate modes from the surface-normal direction(Fig. 3). Holographic couplers can be made from silver halide, dichromated gelatin (DCG) films and from photopolymer holographic recording films. Silver halide suffers from lower resolution and higher scatter. DCG has excellent holographic performance (high index modulation) and low scatter. However, DCG is seriously affected by raw material variability, requires complex wet processing and final holograms must be hermetically sealed to ensure environmental stability[5]. Photopolymer films do not require wet processing and particular means to protect the finished hologram and it is easier to use and handle.

Volume phase holograms are formed in the photopolymer material through optical recording which produces a spatial variation in refractive index. The sinusoidal index of refraction variation in the photopolymer material is generated by the diffusion and migration of photosensitive monomers and the subsequent fixing of these monomers. According to Kogelnik's coupled wave theory[6] for thick hologram gratings, the efficiency of a volume transmission grating is a sinusoidal function of the product of grating thickness and index modulation. By selecting the proper thickness for a holographic film with a given index modulation, large than 99% diffraction efficiency has been realized for a desired reconstruction wavelength. Further increase in film thickness results in lower diffraction efficiency, a condition referred to as overmodulation..Diffraction efficiency can be controlled by varying the photo-exposure dosage or the ratio of the two interference beams[7]. To achieve such a fine tuning on the diffraction efficiency, a thorough understanding of the photopolymer film characteristics is necessary.

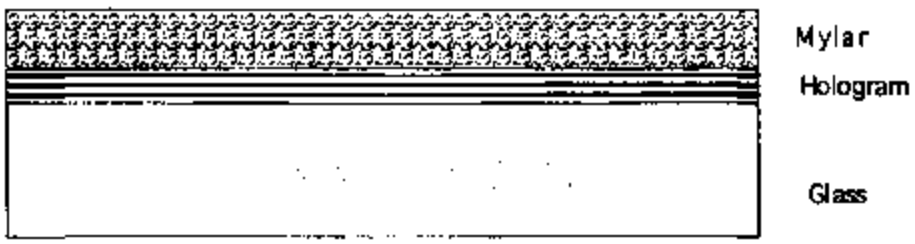

Figure 4 Structure of the holographic grating

The photopolymer films typically consist of polymeric binders, acrylic monomers, and plasticizers, along with initiating systems including initiators, chain transfer agents, and photosensitizing dye. The binder acts as the support matrix containing other film components. The monomers serve as refractive index "carriers". The holographic photopolymer is usually coated from solvent onto a clear support, a 50 μm Mylar® polyester film. A removable cover sheet of 25 μm Mylar film is used to protect the slightly tacky photopolymer. The film can be used for holographic recording by removal of the cover sheet and lamination of the film to a glass plate or directly to a master plate as depicted in Fig. 4.

HRF-600 film has been specially formulated for transmission holograms and is much less sensitive to fringe spacing. Hologram recording process consists of exposure, UV cure, and heat processing.

Figure 5 is a typical set-up for making holographic gratings on photopolymer structures illustrated in Fig.4. A two beam interference recording method is used to define individual holographic gratings, each

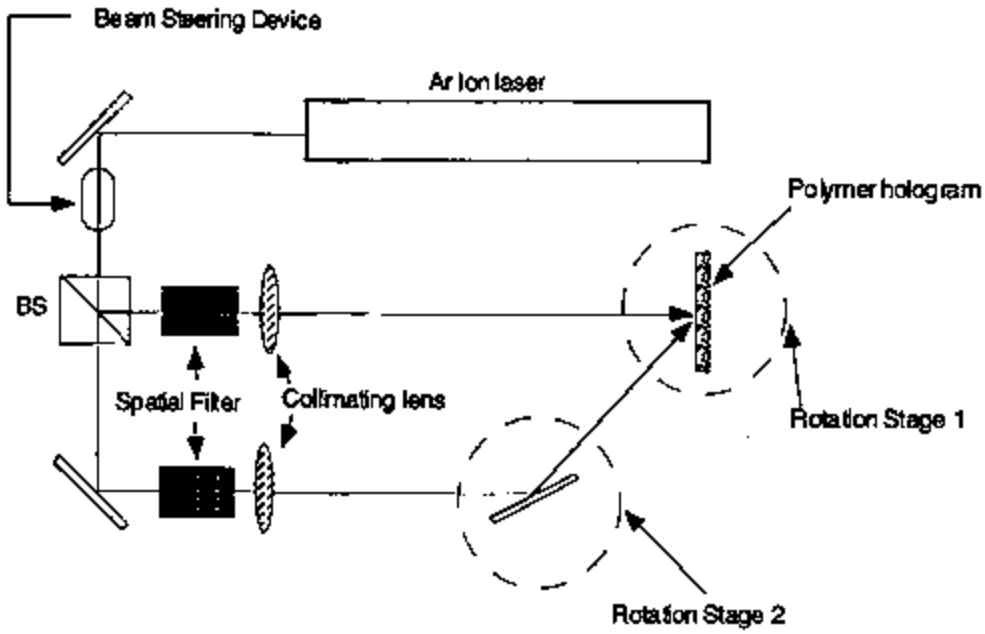

Figure 5. Set-up for making holographic grating couplers

at different recording angles. The 514 nm line from an Argon ion laser is used as the recording wavelength. The laser output is first split into two separate beams, which are spatially filtered and collimated respectively. Then they are designed to intersect on the photopolymer film with specific angles. These angles determine the grating periodicity and the slant angle with respect to the surface normal of the film. The substrate bouncing angle and the diffraction efficiency depend critically on these two angles. Both types of hologram gratings are created by successively exposing holographic patterns within the selectively defined and sensitized regions of the polymer film.

Design of holographic gratings is accomplished by constructing a grating vector such that a specific phase matching condition can be met. Notice that a particular design is for operation at a specfic Bragg diffraction angle and a specific display wavelength. To form a slanted grating coupler which converts a vertical incident wave to a TIR with bouncing angle α in the substrate, the two incident angles of the recording beam with respect to the surface normal of the film are[8]

$$\theta_1 = \sin^{-1}\left\{\frac{n}{n_r}\sin\left[\frac{\alpha}{2}+\sin^{-1}\left(\frac{\lambda_b}{\lambda_r}\sin\left(\frac{\alpha}{2}\right)\right)\right]\right\},$$

and (8)

$$\theta_2 = \sin^{-1}\left\{\frac{n}{n_r}\sin\left[\frac{\alpha}{2}-\sin^{-1}\left(\frac{\lambda_b}{\lambda_r}\sin\left(\frac{\alpha}{2}\right)\right)\right]\right\};$$

where n is the average refractive index of the holographic material, n_r is the refractive index of the medium on top of the holographic emulsion (n_r=1 for air), λ_h and λ_r represent the wavelengths of the recording and display (reconstruction) waves, respectively.

Due to the slanted nature of the grating and to the difference in refractive index between the polymer film and the medium above it, the range of α is limited. To increase α, i.e., increase the bouncing distance of the substrate mode, we can either decrease the ratio of λ_h/λ_r by changing the recording and reconstruction wavelength ot increase n_r by putting a high index prism right in front of the holographic emulsion area during recording.

6. OPTICAL FANOUT BEAM UNIFORMITY

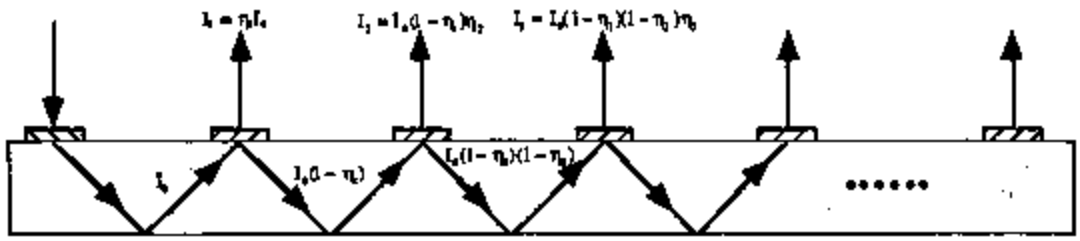

Figure 6 Light intensity at various substrate mode guided positions and on different output couplers

Uniform fan out intensity is required for a practical system. To ensure that the fanout optical signals from each output coupler are uniform in intensity, it is necessary to fine tune the diffraction efficiency from each output couplers. Let us examine the diffraction efficiency distribution for an one-dimensional array. As illustrated in Fig. 6, intensity uniformity requires that

$$\left.\begin{aligned} &I_0\eta_1 = I_0(1-\eta_1)\eta_2 \\ &I_0(1-\eta_1)\eta_2 = I_0(1-\eta_1)(1-\eta_2)\eta_3 \\ &I_0(1-\eta_1)(1-\eta_2)\eta_3 = I_0(1-\eta_1)(1-\eta_2)(1-\eta_3)\eta_4 \end{aligned}\right\} \Rightarrow \quad \begin{aligned} \eta_2 &= \frac{\eta_1}{1-\eta_1} \\ \eta_3 &= \frac{\eta_2}{1-\eta_2} = \frac{\eta_1}{1-2\eta_1} \\ \eta_4 &= \frac{\eta_3}{1-\eta_1} = \frac{\eta_1}{1-3\eta_1} \end{aligned} \qquad (9)$$

In general,

$$\eta_k = \frac{\eta_{k-1}}{1-\eta_{k-1}} = \frac{\eta_1}{1-(k-1)\eta_1} \qquad k = 1,2,3,\ldots\ldots,N \qquad (10)$$

Depending on the value of N and the maximum diffraction efficiency achievable for an individual holographic grating, we can determine all the different diffraction efficiencies η_k (k=1,2,..., N). For example, if N=8, and assuming that $\eta_8 = 90\%$, we can obtain the different diffraction efficiencies η_k for k=1,2,..., 7. Specifically, they are $\eta_1 = 12.3\%$, $\eta_2 = 14\%$, $\eta_3 = 16.3\%$, $\eta_4 = 19.5\%$, $\eta_5 = 24.2\%$, $\eta_6 = 32\%$, $\eta_7 = 47\%$. This diffraction distribution is shown in Fig. 7 below.

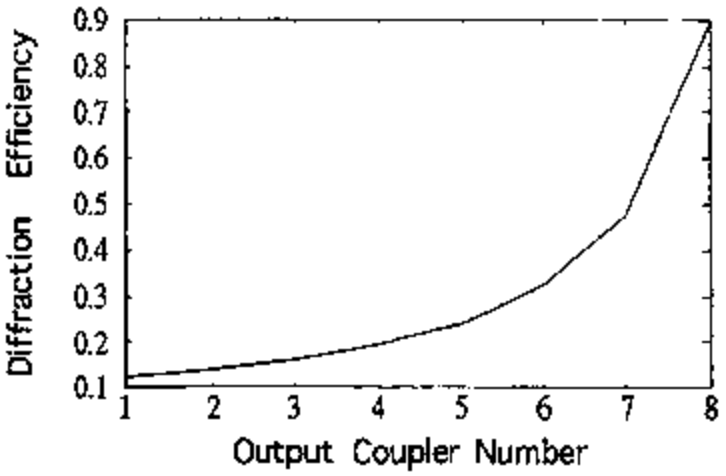

Figure 7 Diffraction efficiencies for the output grating couplers to generate 1-to-8 fanout

7. EXPERIMENTAL RESULTS

With the coherent mixing of two CW lasers oscillating at single longitudinal frequencies, microwave frequency rf signals can be generated by optical heterodyne techniques. We employed two tunable diode lasers with a lasing wavelength around 786 nm. As indicated in Fig. 8, the outputs of the lasers are combined by a 50:50 beam splitter, passing an optical isolator and then coupled into the waveguide by a prism coupler at a suitable angle of incidence. Optical signal is coupled out of the waveguide through another prism coupler and then to a single mode fiber (SMF) with a 20 X microscope objective lens. The output of the fiber is launched directly to an ultrafast photodetector with 60 GHz bandwidth through thematched FC connector. The PD output is amplified through a broadband amplifier and immediately connected to a spectrum analyzer for display. The photocurrent output from the PD contains a DC part and an AC part corresponding to the high frequency rf beat signal. If the optical fields of two separate lasers are given by $E_1 = A_1 \exp(j\omega t)$ and $E_2 = A_2 \exp\{j(\omega + \omega_{12})t\}$, where ω_{12} is the beat frequency and the two lasers are linearly polarized in the same direction. The output of the photodetector in the form of photocurrent is therefore given by [9]

$$i_c(t) = \frac{e\eta}{h\nu}(A_1^2 + A_2^2 + 2F(\omega_{12})A_1A_2\cos(\omega_{12}t)). \qquad (11)$$

Here, e is the electron charge, η is the quantum efficiency of the detector, $h\nu$ is the incoming photon

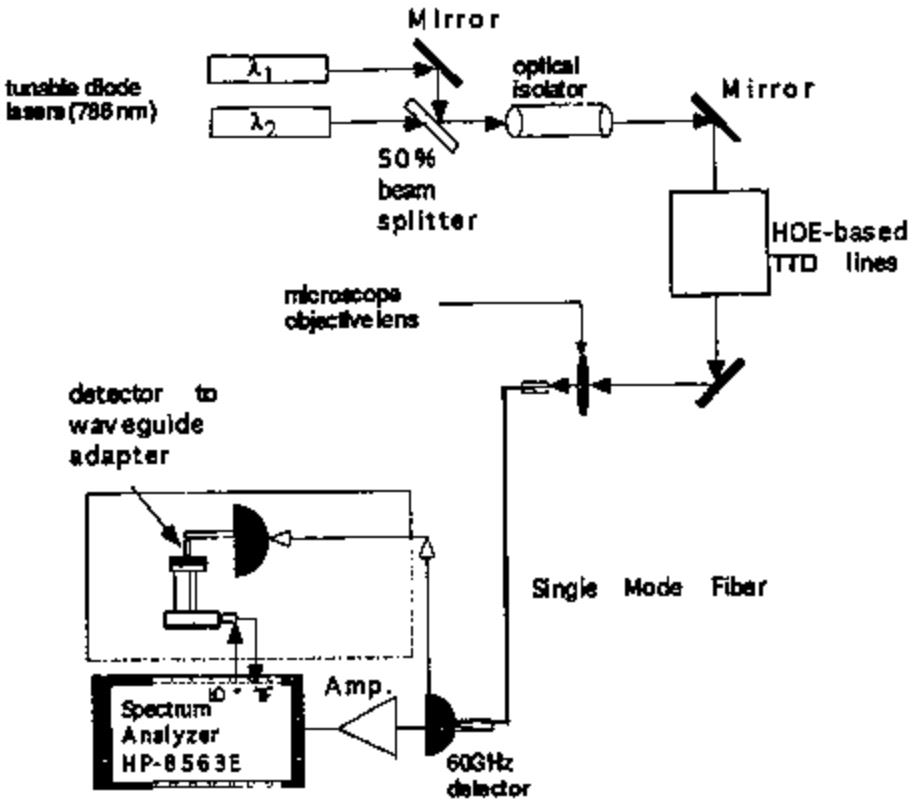

Figure 8. Set-up of the generation of microwave signals by optical heterodyne detection.

energy and $F(\omega_{12})$ is the frequency response function of the PD. The optical-to-electrical conversion represented by Eq.(11) is equivalent to that of directly modulating a laser diode.

With the set-up of Fig. 8, we have successfully produced and detected microwave frequency signals from 1 GHz up to the 25 GHz band. Figure 9 shows the detected 25 GHz rf signal by an spectrum analyzer. A signal to noise (S/N) ratio of ~ 20 dB is obtained. Presently, 25 GHz is limited only by the frequency response of the amplifier and the spectrum analyzer used. Realizing the fact that a small tuning of the laser wavelength (a few A°) will provide a large beat frequency, the task of generating wideband rf signals up to 60 GHz will be reported in the near future. In fact, microwave signals as high as several hundred gigahertz has already been achieved, only hindered by the difficulties of detecting and demonstration of such signals. By using external mixers and wideband amplifier, much higher upper frequency[10] is expected. Feasibility of manipulating the HOE arrays shown in Fig. 3 with an accurate diffraction efficiency is further studied experimentally. Figure 10 illustrates a massive fanout containing 30 delay lines using multiplexed holographic grating couplers developed. For the purpose of demonstration, the display wavelength in this figure is 514 nm. Each fanout beam is provided through the corresponding Bragg diffraction. The total diffraction efficiency is 92% with power fluctuation within ±3% among all 30 fanout beams.

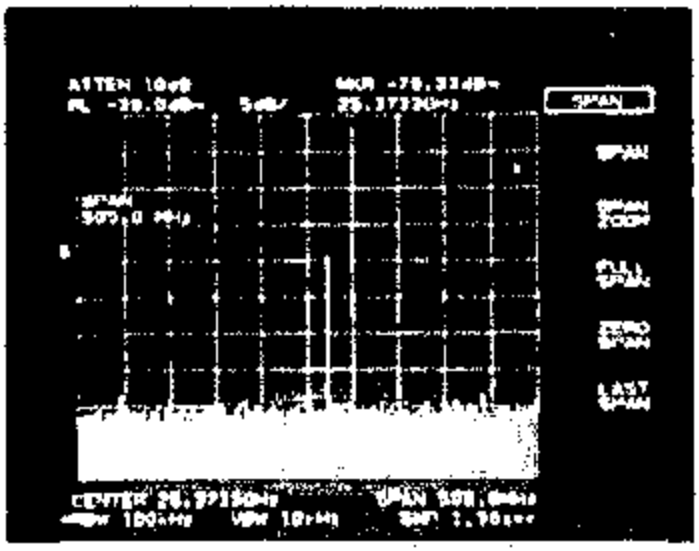

Figure 9 25 GHz Optical heterodyne signal detected by spectrum analyzer

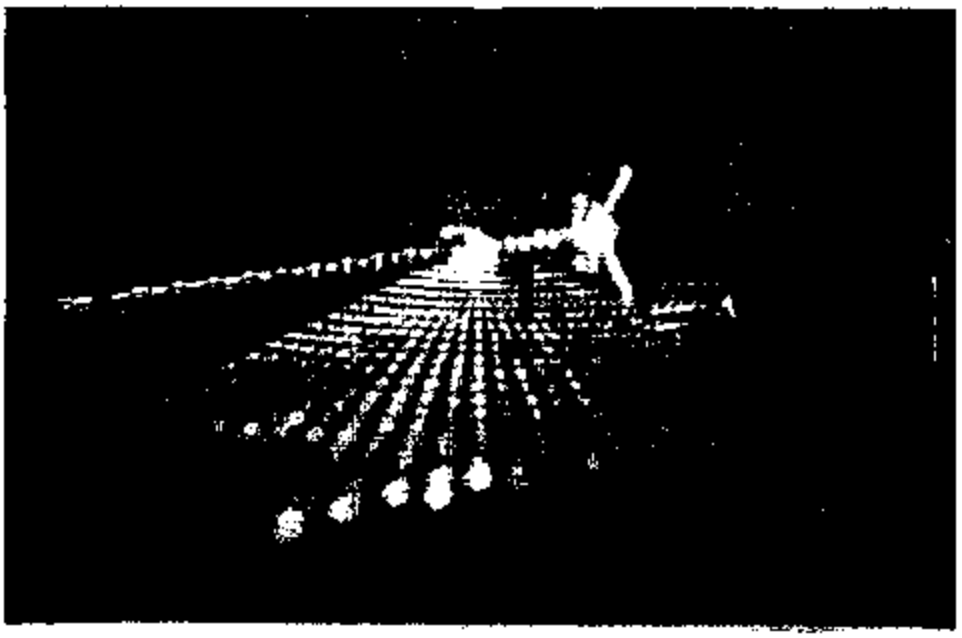

Figure 10 1-to-30 massive substrate mode optical fanout

8. ACKNOWLEDGEMENTS

This research is currently supported by the Office of Naval Research. The authors thank Dr. Y. S. Park for his encouragement. Technical discussions with Dr. W. Ng of Hughes Research Lab is also acknowledged.

9. REFERENCES

[1] H. Zmuda and E.N. Toughlian, "Photonic Aspect of Modern Radar", Artech House, 1994

[2] E. Ackerman, et al., *IEEE MTT-S Digest*, **R-6**, 681(1992).

[3] W. Ng, et al., *IEEE J. of Lightwave Technology*, **9**, 1124(1991).

[4] W. Ng, et al., *Electron. Lett.*, **26**, 791(1990).

[5] R. T. Chen, *Optics and Laser Technology.*, **25**, 347-365(1993).

[6] H. Kogelnik, *The Bell System Technical Journal.*, **48**, 2909(1969).

[7] U. Rhee, et al., *Opt. Eng.*, **32**, 1839(1993).

[8] R. T. Chen, S. Tang, et al. *Appl. Phys. Lett.*, **63**, 1883(1993).

[9] S. Kawanish, A. Takada, and M. Saruwatari, *IEEE J. of Lightwave Technology*, **7**, 1, 92(1989).

[10] R.T. Chen, H. Lu, D. Robinson, Z. Sun, and T. Jannson, *Applied Physics Letters*, **60**, 5, 536(1992).